NASA Technical Paper 1029

Representation of Turbulent Shear Stress by a Product of Mean Velocity Differences

Willis H. Braun

SEPTEMBER 1977

NASA

NASA Technical Paper 1029

Representation of Turbulent Shear Stress by a Product of Mean Velocity Differences

Willis H. Braun

Lewis Research Center
Cleveland, Ohio

National Aeronautics
and Space Administration

**Scientific and Technical
Information Office**

1977

CONTENTS

REPRESENTATION OF TURBULENT SHEAR STRESS BY A PRODUCT OF MEAN VELOCITY DIFFERENCES

by Willis H. Braun

Lewis Research Center

SUMMARY

A simple argument leads to the proposal of a quadratic form in the mean velocity for the turbulent shear stress. The proposed form is expressed as the product of two velocity differences whose roots are the maximum velocity in the flow and a "cutoff" velocity below which the turbulent shear stress vanishes. Application to pipe and channel flows yields the centerline velocity as a function of pressure gradient, as well as the velocity profile. The flat-plate, boundary-layer problem is solved by a system of integral equations to obtain the friction coefficient, the displacement thickness, and the momentum-loss thickness. Comparisons are made with experiment.

INTRODUCTION

Theories of turbulence are generally classified according to the number of partial differential equations that must be solved in conjunction with the Reynolds equation for the time-mean flow (Reynolds, ref. 1; Launder and Spalding, ref. 2). If one additional equation (e.g., an equation for the turbulent kinetic energy) must be solved, the theory is called a one-equation model; if, beyond that, a differential equation for the characteristic length of the turbulent motions must be solved, the theory is called a two-equation model; and so forth.

The move toward more elaborate treatments of turbulent flows arises from the failure of the zero-equation models, that is, those which model turbulent stresses with an algebraically specified relation to the mean-flow quantities, to prove both general and accurate. The zero-equation theories have been constructed almost exclusively upon the hypothesis of Boussinesq (ref. 2) that the stress should be modeled as a product of an eddy viscosity and the mean-velocity gradient in the manner of Newton's law for viscous fluids. Various forms of this hypothesis have been successful in describing a wide variety of flows of practical importance. Nevertheless, it is now generally agreed

(Townsend, ref. 3, p. 107; Tennekes and Lumley, ref. 4, ch. 2) that this hypothesis does not have a firm physical base. Its most successful form, the mixing-length theory, requires a supplement of empirical information and theoretical modification (ref. 2, lecture 2), which diminishes the confidence with which it can be transferred from one type of flow to another.

The question that is asked and explored in this report is whether an alternative zero-equation model of turbulence can be constructed by formulating a hypothesis for stress that is compatible with its known physical and mathematical properties and that retains simplicity of form by relying on a minimum of empirical constants and functions. Elementary observations are shown to lead to a simple expression for stress that approximates closely the distribution found in several common types of flow. The stress formula is applied to channel and pipe flows to find the velocity profiles and the variation of centerline velocity with pressure gradient. By using an approximate velocity profile in a system of integral equations, the friction coefficient, displacement thickness, and momentum-loss thickness in a flat-plate boundary layer are found. Comparisons are then made with experiment.

HYPOTHESIS FOR TURBULENT SHEAR STRESS

A hypothesis for turbulent stress should meet a number of requirements if it is to be a valid candidate for consideration and use in actual calculations. It should, first of all, lend itself to expression mathematically as a tensor inasmuch as the stress itself is a tensor. If only one component of the stress (e.g., the shear component) is being considered, it should be formulated in a way that could conceivably be generalized to a tensor of order 2. Second, it should be expressed as a function only of the dynamic variable of the problem it is to be used in, namely, the time-mean velocity, its derivatives, and, possibly, its integrals. Finally, it should express the experimental fact (ref. 4) that the stress has a nonlocal character and that its value at any point depends not on the dynamic variable or its derivatives at that point alone, but on conditions at other points in the flow as well.

As a restriction to problems of a simple yet practical sort, we confine our remarks to nearly unidirectional flows, steady and incompressible, whose lateral extent is much less than the extent in the streamwise direction. Among these are flows in pipes and channels, boundary layers, wakes, and jets. The velocity component in the direction of flow is $U(Y)$. (Symbols are defined in appendix A.)

It is convenient to begin by considering the integrated frictional drag force on a body. A very elementary property of turbulent drag is that it is closely proportional to the square of the undisturbed velocity of the stream. While it is true that in boundary-layer and pipe flows, for example, this behavior is modified by a weak

Reynolds number dependence, such deviation can be ascribed to the presence of viscosity rather than to the turbulent motions themselves. Not only is the square of the velocity descriptive of the drag in a quantitative way, it is also dimensionally appropriate when combined with the other available dimensional quantities, the density of the fluid and the characteristic dimension of the body. This suggests that at any point in the flow a component of stress may be related to the square of the local mean velocity. Further, if the shear stress, which is the component of interest here, were approximated by a polynomial of arbitrary power in the velocity, it would need to have no more than two roots since it vanishes only twice: once at the maximum mean velocity, and once at or near the minimum velocity in the flow.

All of these considerations make it plausible to model the turbulent shear stress by a quadratic form in the local mean velocity,

$$\tau = \rho(AU^2 + BU + C) \tag{1}$$

If the two roots are located at the maximum velocity U_m and at some "cutoff" velocity U_c below which the shear stress vanishes, then

$$\tau = \alpha\rho(U_m - U)(U - U_c) \tag{2}$$

where α is a pure number that should be independent of mean-flow quantities. The quadratic form (eq. (2)) is, perhaps, the simplest hypothesis that could be made for the turbulent shear stress and has the additional property that it resembles the definition of Reynolds stress as a time-averaged product of fluctuating velocities by exhibiting a product of mean-velocity differences. It also has the desired appearance of a component of a second-order tensor, especially if α were the component of a fourth-order tensor. In a very limited sense it is even a nonlocal description of the stress, introducing the velocities U_m and U_c at points other than that at which the stress is being calculated.

Actually, of course, any point in the flow is connected with almost all other points across the local cross section by the turbulent motions, so equation (2) should be thought of as a first approximation to the most general description of this sort.

The conic section described by equation (2) is a parabola in the mean velocity. Whether or not this is descriptive of the experimentally observed shear stress can be judged by comparing the hot-wire measurements of shear stress in flows of the type being considered here with parabolas fitted to them on the basis of least square error. This has been done in figure 1. The circular symbols represent actual hot-wire measurements or points from curves faired through hot-wire meauurements. The square symbols are values derived from mean-velocity data, either by estimating the cutoff velocity or by measuring the profile slope. The parabolas are required in each case to pass through the point of symmetry, $U/U_m = 1$, $\tau = 0$.

The agreement between the experimental data and the least-squares parabolas is sufficiently good that the error in using the latter would not be a large fractional part of the true value for flows bounded by walls, namely, boundary layers and pipe and channel flows. However, for free turbulent flows, the half jet and the wake, the agreement is not as good. The parabola is successful in representing the stress as obtained indirectly from mean-velocity measurements, but these data are not in agreement with the stress as measured directly by hot wire. The right leg of the parabola for the wake, which corresponds to the center of the wake, may yield a shear stress that is too small.

This latter point is emphasized by wake measurements of Chevray and Kovasznay (ref. 5), which are shown in figure 2. (Data are presented in ref. 6.) At the center of the wake, the slope of the data is nearly infinite and the parabola, which is chosen to pass through the points $\tau = 0$, $(U_e - U)/(U_e - U_0) = 0, 1$, cannot accurately represent the stress in the center region. (U_e and U_0 are the velocities at the edge and center of the wake, respectively.)

On the basis of these observations the stress hypothesis (eq. (2)) will be used subsequently to solve the full boundary-value problem for only those flows that are bounded by walls, although in the following section it will be used to find similarity laws for free turbulent flows as well.

One result of the comparison of hypothesis with experiment in figure 1 is the appearance of a small but finite region of the flow, corresponding to $0 \leq U \leq U_c$, in which the shear stress vanishes. Although the hypothesis does not require that this thin layer of flow be steady and, therefore, laminar, it does state that in it, for all practical purposes, the random fluctuations of velocity are uncorrelated. (However, the correlation of velocity and temperature fluctuations apparently does not always vanish over a finite region. This was shown by the calculations of Deissler (ref. 7) for high Prandtl number.) The appearance of a region of zero stress in this hypothesis corresponds to the influence of viscous damping functions in the eddy diffusivity of Deissler (ref. 7) and the mixing length of van Driest (ref. 8).

The two adjustable parameters of the hypothesis are α and U_c. The coefficient α occupies a position analogous to that of viscosity in viscous stress and should depend only upon the character of the turbulent motions; that is, it may be depend upon the geometry but not upon any dynamic parameter (imposed pressure gradient, free-stream velocity) that might be represented in the product of velocity differences. It may show dependence on preturbulence, free-stream turbulence, and so forth.

The cutoff velocity, for flows bounded by walls, is in the region dominated by the skin friction and, in general, should be a function of the friction coefficient. The function itself should change little from one bounded flow to another. In the calculations to be undertaken subsequently, the functional dependence will be taken as the simplest kind. In figure 3 is shown a sketch of the velocity distribution near the wall in the familiar u^+, y^+ coordinates. The cutoff velocity occurs at the juncture of the profile of

the turbulent region with the line $u^+ = y^+$, which characterizes the sublayer, in which only viscous stresses occur. It is assumed here that, for all flows of one class, the cutoff velocity $u_c^+ = U_c/U_\tau$ will be a constant. The constant will be allowed to vary from class to class, but all pipe flows will have the same value of u_c^+, all channel flows their own characteristic value, and so forth.

SIMILARITY LAWS

An immediate test that can be applied to the hypothesis (eq. (2)) is a comparison of the similarity laws that it predicts with those encountered experimentally. In deriving the similarity laws one assumes that the viscous stresses may be neglected compared with the turbulent stresses. The similarity laws predicted by the shear-stress hypothesis for plane and circular wakes, plane and circular jets, and the half jet are derived in appendix B. The results are shown in the following table:

Flow	Width	Centerline velocity or velocity deficit
Plane jet	X	$X^{-1/2}$
Circular jet	X	X^{-1}
Plane wake	$X^{1/2}$	$X^{-1/2}$
Circular wake	$X^{1/3}$	$X^{-2/3}$
Half jet	X	X^{0}

These are exactly the laws derived from the mixing-length theory and confirmed by experiment (Schlicting, ref. 9).

The partial differential equation that governs the half jet is also appropriate to the outer portion of the flat-plate boundary layer. Consequently, the outer portion of that boundary layer should have Y/X as a similarity variable for the velocity profiles. This was confirmed experimentally by Townsend (ref. 10).

CHANNEL FLOW

As a first application and test of the hypothesis for turbulent stress, consider fully developed flow between infinite parallel walls of spacing $2D$ (fig. 4). There is no acceleration of the fluid, so the pressure gradient and retarding forces are in balance. The maximum velocity U_m occurs at the centerline, so we may write for the fluid in the upper half of the channel

$$\frac{\partial}{\partial Y}\left[\mu \frac{\partial U}{\partial Y} - \alpha\rho(U_m - U)(U - U_c)\right] = \frac{\partial P}{\partial X} \qquad \text{for } U_c < U < U_m \tag{3a}$$

and

$$\mu \frac{\partial^2 U}{\partial Y^2} = \frac{\partial P}{\partial X} \qquad \text{for } 0 < U < U_c \tag{3b}$$

where the lateral coordinate Y is measured from the channel centerline.

If the reference velocity is chosen to be the maximum velocity that the fluid would have in laminar flow, namely,

$$U_r \equiv \frac{D^2}{2\mu}\left|\frac{\partial P}{\partial X}\right|$$

and if the half width D is chosen as the standard of length, equation (3a) after one integration and equation (3b) after two integrations become

$$\frac{du}{dy} - \alpha p(u_m - u)(u - u_c) = -2y \qquad \text{for } u_c < u < u_m \tag{4a}$$

and

$$u = 1 - y^2 \qquad \text{for } 0 < u < u_c \tag{4b}$$

The new parameter, p, is the dimensionless pressure gradient or, equivalently, the Reynolds number based on the reference velocity,

$$p \equiv \frac{U_r D}{\nu} \equiv \frac{D^3}{2\mu\nu}\left|\frac{\partial P}{\partial X}\right| \tag{5}$$

Equation (4b) states that the velocity in the sublayer follows the parabolic distribution that it would have in a laminar flow at the same pressure gradient (ref. 3, fig. 9.1). Equation (4a) is a Riccati equation (Goldstein and Braun, ref. 11) that can be transformed[1] to the Airy equation in the following manner: The velocity deficit $w \equiv u_m - u$ is replaced by a variable W through

[1]This transformation was pointed out to the author by Dr. M. Goldstein.

$$w = -\frac{1}{\alpha p}\frac{W'}{W}$$

There follows a second-order equation

$$W'' + \alpha p w_c W' + 2\alpha p y W = 0$$

which, in turn, is transformed by $W = e^{sy}T(y)$ to

$$T'' + (2s + \alpha p w_c)T' + \left(s^2 + \alpha p w_c s + 2\alpha p y\right)T = 0$$

with

$$w_c \equiv u_s - u_c \tag{6}$$

The first derivative can be eliminated by choosing

$$s = -\frac{\alpha p w_c}{2}$$

so that

$$T'' + \left[2\alpha p y - \left(\frac{\alpha p w_c}{2}\right)^2\right]T = 0$$

Introducing a new independent variable x defined by

$$x = -\sqrt{a}y + \left(\frac{a w_c}{4}\right)^2 \tag{7}$$

where

$$a \equiv (2\alpha p)^{2/3} \tag{8}$$

leads to the Airy equation

$$\frac{d^2T}{dx^2} - xT = 0 \tag{9}$$

In terms of the dependent variable T, the velocity deficit is

$$w = \frac{2}{a}\left(\sqrt{x_m} + \frac{1}{T}\frac{dT}{dx}\right) \tag{10}$$

where

$$x_m \equiv \left(\frac{aw_c}{4}\right)^2 \tag{11}$$

is the value of x at the origin of y.

The most general solution of the differential equation (9) is

$$T = c_1 Ai(x) + c_2 Bi(x) \tag{12}$$

where Ai(x) and Bi(x) are Airy functions (Abramowitz and Stegun, ref. 12) of the first and second kinds, respectively, and c_1 and c_2 are constants. Because of the form of the expression (10) for the velocity deficit, only the ratio of the constants $k \equiv c_2/c_1$ enters into the solution:

$$w = \frac{2}{a}\left[\sqrt{x_m} + \frac{Ai'(x) + kBi'(x)}{Ai(x) + kBi(x)}\right] \tag{13}$$

The coordinate x has its origin at a point near the wall where the total stress ($2y = \tau_t D/\mu U_r$ in dimensionless form) is equal to the maximum $\alpha p(w_c/2)^2$ that the turbulent stress alone reaches in the flow. The coordinate of the cutoff velocity is obtained by combining equations (4b), (7), and (11), which yields

$$x_c \equiv x_m - \sqrt{a(1 - u_c)} \tag{14}$$

At the center of the channel the velocity deficit vanishes to give

$$k = -\frac{Ai'(x_m) + \sqrt{x_m}Ai(x_m)}{Bi'(x_m) + \sqrt{x_m}Bi(x_m)} \tag{15}$$

The boundary condition at x_c is

$$w_c = \frac{2}{a}\left[\sqrt{x_m} + \frac{Ai'(x_c) + kBi'(x_c)}{Ai(x_c) + kBi(x_c)}\right] \tag{16}$$

which, combined with equation (11) to eliminate w_c, yields a second expression for k,

$$k = -\frac{Ai'(x_c) - \sqrt{x_m}Ai(x_c)}{Bi'(x_c) - \sqrt{x_m}Bi(x_c)} \tag{17}$$

Equating the two expressions for k relates the coordinate values x_m and x_c of the two velocities u_m and u_c. The relation may be expressed in a simpler form by noting that estimates from experiment show

$$\left.\begin{aligned} x_m &= O(10) \\ x_c &= O(1) \end{aligned}\right\} \tag{18}$$

Then, since for $x > 2$, $Ai'(x), Ai(x) \ll Bi'(x), Bi(x)$, it follows from the first expression for k (eq. (15)) that

$$k \ll 1 \tag{19}$$

and from the second expression for k (eq. (17)) that the relation between x_m and x_c is approximately

$$\sqrt{x_m} = \frac{Ai'(x_c)}{Ai(x_c)} \tag{20}$$

Introducing equations (11) for x_m and (14) for x_c, supplemented by equation (8) for a, yields a relation among u_m, u_c, and p. The cutoff velocity can be eliminated because we have set u_c^+ = Constant and, by definition,

$$u_c^+ \equiv \frac{U_c}{U_\tau} = \frac{U_c}{U_r}\frac{U_r}{U_\tau} = u_c\sqrt{\frac{p}{2}}$$

or

$$u_c = u_c^+ \sqrt{\frac{2}{p}} \tag{21}$$

The resulting dependence of centerline velocity u_m on the pressure gradient p is plotted in figure 5, where it is compared with the experimental data of Laufer (ref. 13). The values of α and u_c^+ that were found by trial to provide a good fit were 0.01 and 6, respectively. The agreement between theory and experiment is good, the maximum difference being at the high values of pressure gradient, where it is about 6 percent.

The dimensionless average velocity through the channel, defined as

$$\bar{u} \equiv \frac{\int_0^D U \, dY}{U_r D} = \int_0^1 u \, dy$$

can be found from equations (13) and (4b) to be

$$\bar{u} = \frac{u_m + u_c}{2} y_c + \frac{2}{a^{3/2}} \ln \frac{Ai(x_c) + kBi(x_c)}{Ai(x_m) + kBi(x_m)} + \frac{2 - y_c(2 + u_c)}{3}$$

where

$$y_c \equiv \sqrt{1 - u_c}$$

This quantity is also shown in figure 5. The ratio $\bar{u}/u_m$ approaches 1 as the pressure gradient becomes very large.

In figure 6 a velocity profile at a Reynolds number ($Re = pu_m$) corresponding to one of those at which Laufer's measurements were taken is compared with the experimental profile. The theoretical profile is not as full as the experimental profile, and this must be ascribed to a failure of the stress hypothesis to provide a sufficiently strong stress in the center of the channel. Nevertheless, because the centerline velocity is predicted accurately, the mean velocity is not likely to be in substantial error.

PIPE FLOW

The momentum equation for fully developed pipe flow is (Laufer, ref. 14)

$$\frac{1}{\rho} \frac{dP}{dX} = \frac{1}{R} \frac{d}{dR} R \frac{\tau}{\rho} + \nu \left(\frac{d^2U}{dR^2} + \frac{1}{R} \frac{dU}{dR} \right) \tag{22}$$

where, as usual, X and R are the axial and radial coordinates, respectively. Introducing equation (2) and nondimensionalizing the radius of the pipe R_0 and the centerline velocity for laminar flow

$$U_R = \frac{R_0^2}{4\mu}\left|\frac{dP}{dX}\right| \tag{23}$$

yield

$$\frac{du}{dr} - \alpha p_0(u_m - u)(u - u_c) = -2r \tag{24}$$

where

$$p_0 \equiv \frac{U_R R_0}{\nu} \equiv \frac{R_0^3}{4\mu\nu}\left|\frac{dP}{dX}\right| \tag{25}$$

$$r = \frac{R}{R_0} \tag{26}$$

The reference velocity (eq. (23)) is just one-half that for a channel flow with its half-width equal to the pipe radius; the factor 1/2 is also reflected in the definition of the dimensionless pressure gradient (eq. (25)).

Equation (24) governing the flow is identical to the Riccati equation treated for channel flow, and the solution proceeds in exactly the same way. Figure 7 shows the dependence of the dimensionless centerline velocity upon the dimensionless pressure gradient p_0 as compared with the experimental data of Laufer (ref. 14) and Sandborn (ref. 15). The value of the parameter α has been kept at 0.01, but the value of u_c^+ has been raised from 6 to 7 to give the best fit to the experimental data. The calculated curve is slightly above the data at low p and slightly below at high p. Further calculations show that raising u_c^+ above 7 can place the curve through the high-p data and that lowering it can place the curve through the low-p data. It can be concluded, therefore, that the choice of constant u_c^+ is nearly the correct one but that improvement could be obtained with a more general dependence on the parameter p.

Also in figure 7 the dimensionless average velocity

$$u = 2\int_0^1 ru\, dr$$

is compared with the universal resistance law for pipes (Schlicting, ref. 9). The calculated $\bar{u}$ line is nearly parallel to the u_m line, which shows that the calculated velocity profiles do not change with p sufficiently for the mean velocity to follow the observed values closely.

Figure 8(a) shows the velocity profiles at $Re = p_0 u_m$ of 250 000 and 25 000. Just as in the case of channel flow, the calculated profile has the correct overall characteristics but is not as full as the profile found experimentally by Laufer. The same profiles are also given in terms of the similarity variables u^+ and y^+ in figure 8(b). This plot shows both of the effects already observed in figures 7 and 8(a). The calculated profiles tend not to be as full as the observed data, and the centerline velocity is too high at the low dimensionless pressure gradient and too low at high p.

FLAT-PLATE BOUNDARY LAYER

Differential Equations

For a boundary layer the hypothesis for the turbulent stress has the form

$$\tau = \alpha\rho(U_\delta - U)(U - U_c) \qquad \text{for } U_c < U < U_\delta \tag{27}$$

where U_δ is the stream velocity at the edge of the boundary layer. We again assume that the minimum velocity in the turbulent region U_c is given by

$$u_c^+ \equiv \frac{U_c}{U_\tau} = \text{Constant} \tag{28}$$

with $U_\tau \equiv \sqrt{\tau_w/\rho}$ in the customary way.

The stress hypothesis (eq. (27)) is introduced into Prandtl's equation for the incompressible boundary layer

$$U\frac{\partial U}{\partial X} + V\frac{\partial U}{\partial Y} = U_\delta\frac{dU_\delta}{dX} + \nu\frac{\partial^2 U}{\partial Y^2} + \frac{\partial}{\partial Y}\frac{\tau}{\rho} \tag{29}$$

and at the same time the dependent and independent variables undergo the transformation

$$\left.\begin{aligned} U = U_\delta u,\ V = \alpha U_\delta v \\ X = Lx,\ Y = \alpha Ly \end{aligned}\right\} \tag{30}$$

where L is a typical length for the geometry and u, v, x, and y are considered to be O(1).

Since $\alpha = 0.01$ approximately, judging from experience with the pipe and channel, transformation (3) states that a boundary layer should be about 100 times as long as it is thick. This is in accordance with observation. Prandtl's equation is now

$$u\frac{\partial u}{\partial x} + v\frac{\partial u}{\partial y} = \frac{1}{U_\delta}\frac{dU_\delta}{dx}(1 - u^2) + \frac{1}{\alpha^2\,\mathrm{Re}}\frac{\partial^2 u}{\partial y^2} + \frac{\partial}{\partial y}(1 - u)(u - u_c) \qquad \text{for } u_c < u < 1 \tag{31}$$

where a local Reynolds number

$$\mathrm{Re} \equiv \frac{U_\delta L}{\nu} \tag{32}$$

has been introduced. In this form of the equation, the inertia terms and the turbulent stress terms are of the same magnitude, but the viscous term has a small coefficient. This is in keeping with the well-known property of turbulent boundary layers that the viscous forces are appreciable near the surface, where the velocity derivative is high, although the turbulent stresses dominate throughout most of the boundary layer.

The continuity equation $\partial U/\partial X + \partial V/\partial Y = 0$ becomes under the transformation (eq. (30))

$$\frac{\partial u}{\partial x} + \frac{\partial v}{\partial y} + \frac{u}{U_\delta}\frac{dU_\delta}{dx} = 0 \tag{33}$$

It will be convenient subsequently to have the properties of the velocity profile near the wall in terms of α and Re. Since the wall stress is given by $\tau_w = (\mu\, dU/dY)_0$, the dimentionless velocity derivative at the wall can be expressed in terms of the friction coefficient $f \equiv 2\tau_w/\rho U_\delta^2$ by

$$\left(\frac{du}{dy}\right)_0 = \alpha\ \mathrm{Re}\,\frac{f}{2}$$

Moreover, Pohlhausen's compatibility condition at the wall (Watz, ref. 16, p. 80), found by evaluating the motion with $u = v = 0$, requires

$$\left(\frac{1}{U_\delta}\frac{dU_\delta}{dx} + \frac{1}{\alpha^2\,\mathrm{Re}}\frac{\partial^2 u}{\partial y^2}\right)_0 = 0$$

Therefore, near the wall,

$$u = \frac{\alpha\,\mathrm{Re}\,f}{2}\,y - \frac{\alpha^2}{2}\frac{d\,\mathrm{Re}}{dx}\,y^2 + \cdots \tag{34}$$

Moments of the Equation of Motion

Solutions to the partial differential equations governing the boundary layer have been found principally in three ways. For a laminar boundary layer, it has been possible to reduce the system to one ordinary differential equation by a similarity analysis, at least for certain pressure distributions. This is not a viable approach for the system described by equations (31) and (33) because in the turbulent boundary layer the viscous stress and the turbulent stress lead to different similarity laws and it is not possible to arrive at an ordinary differential equation. A very direct method, which is as available to the turbulent boundary layer as to the laminar, is numerical integration by a marching technique. It would be necessary to use a smaller grid size in the viscous layer than in the outer, turbulent layer and, in addition, it would be necessary to follow accurately the boundary between the two regions at $u = u_c$. Thus, the marching technique as now practiced for laminar boundary layers, although requiring some modification, is adaptable to the turbulent boundary layer as formulated herein.

The method of solution that will be used here is the integral moment method, in which the equation of motion is multiplied by a weighting function and then integrated over the boundary-layer width to produce an ordinary differential equation in the independent variable x. Accounts of its development and practice are given by Walz (ref. 16) and Tetervin and Lin (ref. 17). Most frequently, the first velocity moment is used to provide an energy equation featuring a dissipation integral. However, Tetervin and Lin derived the most general form of an integral moment equation by using arbitrary powers of u and y, and this generality makes it possible to choose a preferred set of the equations.

The present, brief experience with the pair of equations (31) and (33) has led to a preference for a system of moments in $(\delta - y)^n$, that is, taking moments about the edge

of the boundary layer. A reason for choosing coordinate moments over velocity moments may be seen by considering the zeroth moment of equation (31), which is (ref. 16, p. 87)

$$\frac{d\theta}{dx} + \frac{1}{U_\delta}\frac{dU_\delta}{dx}(\delta^* + \theta) = \frac{f}{2\alpha} \qquad (35)$$

where θ and δ^* are the dimensionless momentum-loss and displacement thicknesses. This equation, the lowest order equation of any moment system, has three dependent variables, θ, δ^*, and f. If the next moment equation to be added is the first velocity moment, a new dynamic variable, the energy thickness, is introduced as an unknown. Thus, from this point of view the system does not close: the number of unknowns always exceeds the number of equations. It seems more appropriate to first add two y-moment equations to equation (35) so that the three equations may be thought of as a system for θ, δ^*, and f and only then, if another equation is required, to add the first velocity-moment equation and the energy thickness to the system.

Moreover, when a system of velocity-moment equations was used to solve the pair of equations (31) and (33), it was found that the system was unstable. This may have been due to the choice of approximate velocity profiles, which have to accompany the moment system, but it is more likely that the cause lies in the high powers of u, which multiply the error for any assumed profile and cause it to grow rather than diminish.

The reason for choosing $\delta - y$ rather than y as the moment arm is one of convenience. A moment in $(\delta - y)^n$ is no more than a linear combination of moments in $y^0, y, \ldots, y^{n-1}, y^n$ and, hence, introduces no new information. However, since moments in y tend to yield more complicated equations than moments in u, any simplification that can be attained is desirable. The derivation of the moment equations in $\delta - y$ is given in appendix C. It is apparent there that a number of terms arising from partial integration vanish at the outer edge of the boundary layer due to the choice of $\delta - y$ for the moment arm. In addition, as a subsequent discussion points out, some suggestions for velocity profiles are expressed in terms of $\delta - y$ and, as a result, integrals of moments in $\delta - y$ are simplified.

As shown by equation (C6) of appendix C, the n^{th} integral moment equation for moments taken around the edge of the boundary layer and for the restricted case of the flat-plate boundary layer is

$$\frac{d}{dx}\int_0^\delta (\delta - y)^n u^2\,dy - \delta_{n,0}\frac{d\delta}{dx} - n\int_0^\delta u^2(\delta - y)^{n-1}\,dy\,\frac{d\delta}{dx} + \delta_{n,0}v(\delta) + n\int_0^\delta (\delta - y)^{n-1}\,uv\,dy$$

$$= -\left[\delta^n\left(\frac{\partial u}{\partial y}\right)_0 + \delta_{n,1} + n(n-1)\int_0^\delta (\delta - y)^{n-2}\,u\,dy\right]\frac{1}{\alpha^2\,\mathrm{Re}} + n\int_{y_c}^\delta (\delta - y)^{n-1}(1 - u)(u - u_c)dy \qquad (36)$$

where $\delta_{n,j}$ is the Kronecker delta.

We shall require explicitly only the first three of these equations, for $n = 0$, 1, and 2. These are

For $n = 0$:

$$\frac{d}{dx}\int_0^\delta u(1 - u)dy = \left(\frac{1}{\alpha^2\,\mathrm{Re}}\frac{\partial u}{\partial y}\right)_0 \qquad (37a)$$

For $n = 1$:

$$\frac{d}{dx}\int_0^\delta (\delta - y)u^2\,dy - \frac{d\delta}{dx}\int_0^\delta u^2\,dy + \int_0^\delta uv\,dy$$

$$= \left[1 - \left(\delta\frac{\partial u}{\partial y}\right)_0\right]\frac{1}{\alpha^2\,\mathrm{Re}} + \int_{y_c}^\delta (1 - u)(u - u_c)dy \qquad (37b)$$

For $n = 2$:

$$\frac{d}{dx}\int_0^\delta (\delta - y)^2u^2\,dy - 2\frac{d\delta}{dx}\int_0^\delta (\delta - y)u^2\,dy + 2\int_0^\delta (\delta - y)uv\,dy$$

$$= \frac{1}{\alpha^2\,\mathrm{Re}}\left[2\int_0^\delta u\,dy - \delta^2\left(\frac{\partial u}{\partial y}\right)_0\right] + 2\int_{y_c}^\delta (\delta - y)(1 - u)(u - u_c)dy \qquad (37c)$$

The zeroth equation is just a special form of equation (35) for a constant stream velocity. It is obtained after writing, in equation (36),

$$v(\delta) = -\int_0^\delta \frac{\partial u}{\partial x}\, dy = -\frac{d}{dx}\int_0^\delta u\, dy + \frac{d\delta}{dx}$$

The zeroth equation is noteworthy for being independent of the form assumed for the turbulent stress; only the viscous stress at the wall enters into it. The $n = 1$ equation, however, contains an integral of the turbulent stress across the turbulent portion of the boundary layer. This integral represents the total force exerted by the plate laterally against the fluid. The equation for $n = 2$ has an integral of the first moment of the turbulent stress; and since the stress peaks close to the wall, this shows that taking the moment about the edge of the boundary layer is once more desirable. It emphasizes the effect of the stress more than if the moment were taken around $y = 0$.

Choice of Velocity Profiles

The integral moment method proceeds by performing the integrals and derivatives in the system (37) on a velocity profile that contains as many free parameters as there are equations in the system. The profile must have the form of equation (34) near the wall; and it is desirable that at the edge, $y = \delta$, of the boundary layer, $\partial^2 u/\partial y^2 = 0$ in agreement with equation (31).

Power-law profile. - One of the most successful representations of the dimensionless velocity has been the form $u = (y/\delta)^{1/e}$, where $e > 1$. Unfortunately, it does not meet the requirements set previously for behavior at the wall and the edge of the boundary layer. The failure at the latter point is not serious; but in order to avoid a singular slope at the wall, we use equation (34) (modified for constant Re) near the wall so that

$$u = \frac{\alpha\, \mathrm{Re}\, f}{2}\, y \qquad \text{for } 0 < u < u_c \tag{38a}$$

$$u = \left(\frac{y}{\delta}\right)^{1/e} \qquad \text{for } u_c < u < 1 \tag{38b}$$

If we again choose u_c by requiring that the boundary between the sublayer and the turbulent region be at a constant velocity on the u^+, y^+ diagram, we find that

$$u_c^+ = \frac{U_c}{U_\tau} = \frac{U_c}{U_\delta}\frac{U_\delta}{U_\tau} = u_c\sqrt{\frac{2}{f}}$$

or

$$u_c = u_c^+\sqrt{\frac{f}{2}}$$

It proves convenient hereinafter to use $\sqrt{f}$ rather than f or to choose as a new variable

$$F \equiv u_c^+\sqrt{\frac{f}{2}} = u_c \tag{39}$$

Then

$$y_c = \frac{J}{F} \tag{40}$$

where

$$J \equiv \frac{\left(u_c^+\right)^2}{\alpha\ \mathrm{Re}} = \text{Constant} \tag{41}$$

The profile (eq. (38a)) becomes

$$u = \frac{F^2}{J}\,y \tag{42}$$

The two parts of the profile (eqs. (38)) must be matched at $u = u_c$, leading to a connection between the three free parameters δ, e, and F of the profile,

$$\delta = \frac{J}{F^{1+e}} \tag{43a}$$

Its differential form is

$$\frac{\dot{\delta}}{\delta} + (\ln F)\dot{e} + (e + 1)\frac{\dot{F}}{F} = 0 \tag{43b}$$

where $\dot{\delta} \equiv d\delta/dx$, and so forth.

In addition to using this relation between the parameters, we shall also use the first two of the moment equations (37). In appendix D it is shown that they yield a system

$$A_{01}\dot{\delta} + A_{02}\dot{e} + A_{03}\dot{F} = B_0 \tag{44a}$$

$$A_{11}\dot{\delta} + A_{12}\dot{e} + A_{13}\dot{F} = B_1 \tag{44b}$$

and we bring equation (43b) into this system by writing it as

$$A_{31}\dot{\delta} + A_{32}\dot{e} + A_{33}\dot{F} = B_3 \tag{44c}$$

with $A_{21} = 1/\delta$, $A_{22} = \ln F$, $A_{23} = (e + 1)/F$, and $B_3 = 0$.

Initial conditions. - The initial conditions for the system (44), however originally specified, must be converted to the parameters δ, e, and F. To illustrate the integral moment methods we shall integrate the flat-plate, boundary-layer system (44) by starting at station 4 of the Wieghardt experiment and using the measurements as given in the report of the Stanford Conference (ref. 18) for starting conditions. At $X = 0.387$ meter, the dimensional momentum-loss thickness $\Theta = \alpha L\theta$ is 0.0924 centimeter and the friction coefficient f is 0.00364, where $L \equiv 5$ meters is the length of the plate.

The initial condition for F comes from equation (39). According to appendix D,

$$\theta = J\left(\frac{1}{2} - \frac{F}{3}\right) + \delta e\left(\frac{1 + F^{e+1}}{e + 1} - \frac{1 - F^{e+2}}{e + 2}\right) \tag{45a}$$

which, combined with equation (43a), yields

$$\frac{1}{2} - \frac{F}{3} + \frac{e}{F^{e+1}}\left(\frac{1 - F^{e+1}}{e + 1} - \frac{1 - F^{e+2}}{e + 2}\right) - \frac{\Theta}{\alpha LJ} = 0 \tag{45b}$$

as an initial condition for e. The remaining initial condition for δ follows from equation (43a).

Three-parameter profile. - A velocity profile introduced by Pai (refs. 19 and 20) for channel and pipe flows and later adapted by Sandborn (ref. 21) to boundary layers has the form

$$\frac{U}{U_\delta} = A + B\left(1 - \frac{y}{\delta}\right)^2 + C\left(1 - \frac{y}{\delta}\right)^{2e} \tag{46}$$

This is a profile with five parameters that is intended to hold over the entire boundary layer. As in the previous example we shall use this form only in the turbulent region and supplement it with a straight-line profile in the sublayer. We shall also change the square term to a cubic in order that the second derivative vanish at the edge of the boundary layer as required by the equation of motion. To meet the boundary condition at the outer edge of the layer, we set A equal to 1; and to reduce the number of parameters, we match both the values and slopes of the two profile segments at $u = u_c$. The velocity profile is then specified by

$$u = \frac{u_c}{y_c} y \qquad \text{for } 0 < u < u_c \tag{47}$$

where $u_c = F$ and $y_c = J/F$ as before; and

$$u = 1 - b\zeta^3 - c\zeta^{3e} \qquad \text{for } u_c < u < 1 \tag{48}$$

where

$$\zeta \equiv \frac{\delta - y}{\delta - y_c}$$

$$c \equiv \frac{\dfrac{(\delta - y_c)F^2}{3J} - 1 + F}{e - 1}$$

$$b \equiv 1 - F - c$$

Since the matching conditions have determined b and c, only δ, e, and F remain to be determined by the moment equations. Using the moments specified by n of 0, 1, and 2, we again get a system of ordinary differential equations of the form (44) whose coefficients are defined in appendix E.

Calculations

The two systems of moment equations corresponding to the two approximate velocity profiles just described have been integrated, and the results are shown in figure 9. The two-parameter profile can represent the momentum-loss thickness well but, since the two initial conditions were used for θ and f, the displacement-thickness curve shows an error of about 8 percent at the end of the plate. It is apparent that the solutions want to give the flow a constant friction coefficient. This can probably be attributed to the very simple assumption made in choosing the cutoff velocity. A weak dependence of u_c upon f or F might improve the agreement with experiment at the expense, of course, of adding an additional experimental parameter.

The three-parameter velocity profile shows some improvement over the two-parameter profile in the representation of displacement thickness but is hardly otherwise superior.

Figure 10 compares the two velocity profiles with the measured velocity distribution. The velocity measurements and the calculated profiles are plotted against the similarity variable for the outer portion of the boundary layer $\eta = Y/(X - X_0)$, where the virtual origin has been found by trial to be $X_0 = -27$ centimeters. Both profiles have difficulty in duplicating the knee of the curve in the region near the wall. In the case of the power-law profile this can be attributed to the power itself, which instead of ranging from 7 to 9 is approximately 4. Presumably, this is due to the introduction of the straight-line segment in the sublayer. The three-parameter profile follows the cubic term from $y = \delta$ to nearly $y = y_c$ because the value of the exponent e is so large. At that point the third term provides a sharp swing from the cubic curve down to the point $u = u_c, \eta = \eta_c$ at the end of the linear profile of the sublayer. For each case the point u_c, η_c is marked by a heavy dot.

The adjustable parameters α and u_c^+ turn out to be somewhat profile dependent in the case of the boundary layer. For the two-parameter profile the values $\alpha = 0.01$, $u_c^+ = 6$, which were used for the channel, were again employed. However, the values that prove appropriate for the three-parameter profile are $\alpha = 0.0135$ and $u_c^+ = 10$.

CONCLUDING REMARKS

Comparing the calculations with experiment indicates that the stress hypothesis has the proper overall characteristics for describing turbulent flows near walls. The generally correct trends that the theory exhibits are probably attributable to the appearance of the square of the mean velocity in the stress; the lack of precision over a wide range of operating parameters (p or x) lies in the choice of the cutoff velocity. It appears

that the dependence of the cutoff velocity upon the friction coefficient should be refined.

Nevertheless, the variation of cutoff velocity with friction coefficient in the boundary layer, although not precise, is encouraging for the description of the flow near transition and under accelerated free streams. Because the cutoff velocity increases as the square root of the friction coefficient, the theoretical boundary layer will tend to become mostly sublayer whenever the friction is high. This is just the condition observed experimentally near transition and relaminarization. An accurate description under such conditions will require a more flexible profile in the sublayer.

It is not apparent whether the argument that led to the proposed expression for the shear component of stress can be extended to provide the normal stresses as well. Although the normal stresses do not arise in the particular examples discussed herein, it is agreed that they may be important in some flows, in a boundary layer near separation for example, and certainly will be needed for the calculation of pressure distributions. In addition, a representation of other components of the stress may give some clue to the failure of the hypothesis in free turbulent flows.

Lewis Research Center,
National Aeronautics and Space Administration,
Cleveland, Ohio, May 20, 1977,
506-24.

APPENDIX A

SYMBOLS

A, B, C	constants
A_{ij}	matrix coefficients
Ai(x), Bi(x)	Airy functions
Ai', Bi'	derivatives of Airy functions
a	$(2\alpha p)^{2/3}$
B_j	component of column vector
b, c	coefficients in velocity profile
C_i	function of δ, e, and F defined in appendix E
c_i	constant
D	half-width of channel
e	form parameter
F	$u_c^+\sqrt{f/2}$
f	friction coefficient
J	$\left(u_c^+\right)^2/\alpha$ Re
k	constant, c_2/c_1
L	length of flat plate
n	order of moment
P	pressure
p	dimensionless pressure gradient, $U_r D/\nu$
p_0	dimensionless pressure gradient, $U_R R_0/\nu$
R	radial coordinate
R_0	radius of pipe
Re	Reynolds number
r	dimensionless radial coordinate, R/R_0
S_i	function of δ, e, and F defined in appendix E
s	parameter in channel solution

T	intermediate variable in channel solution
U	mean velocity in X-direction
U_c	cutoff velocity
U_m	maximum velocity in flow
U_δ	velocity at edge of boundary layer
U_R	reference velocity for pipe, $R_0^2 \lvert \partial P/\partial X \rvert / 4\mu$
U_r	reference velocity for channel, $D^2 \lvert \partial P/\partial X \rvert / 2\mu$
U_τ	friction velocity, $\sqrt{\tau_w/\rho}$
u, u_c, u_m	dimensionless velocities
u_c^+	U_c/U_τ
$\bar{u}$	average dimensionless velocity
V	velocity in Y-direction
v	dimensionless velocity in y-direction
W	intermediate variable
w	dimensionless velocity deficit, $u_m - u$
w_c	dimensionless velocity deficit, $u_m - u_c$
X, Y	Cartesian coordinates
X_0	virtual origin of boundary layer
x, y	dimensionless Cartesian coordinates
x	independent variable for Airy equation
x_c	value of x at $y = y_c$
x_m	value of x at $y = 0$
y_c	value of y at $u = u_c$
Z, Z_i	variables defined in appendix D
α	adjustable parameter in stress hypothesis
Δ^*	displacement thickness
δ	dimensionless nominal thickness of boundary layer
δ^*	dimensionless displacement thickness
ζ	$(\delta - y)/(\delta - y_c)$
Θ	momentum-loss thickness

θ dimensionless momentum-loss thickness

μ viscosity

ν kinematic viscosity

ρ density

τ turbulent shear stress

τ_t sum of viscous and turbulent shear stresses

τ_w shear stress at wall

APPENDIX B

SIMILARITY LAWS OF JETS AND WAKES.

The equations governing jets and wakes are

$$U\frac{\partial U}{\partial X} + V\frac{\partial U}{\partial Y} = \frac{1}{Y^j}\frac{\partial}{\partial Y}\left(Y^j\frac{\tau}{\rho}\right) \tag{B1}$$

and

$$\frac{\partial}{\partial X}(Y^jU) + \frac{\partial}{\partial Y}(Y^jV) = 0 \tag{B2}$$

where $j = 0$ for plane flows and $j = 1$ for axisymmetric flows.

Jets

Integrating the momentum equation (B1) over the appropriate interval after first multiplying by Y^j yields

$$\int_b^\infty Y^jU\frac{\partial U}{\partial X}\,dY + \int_b^\infty Y^jV\frac{\partial U}{\partial Y}\,dY = \left(Y^j\frac{\tau}{\rho}\right)_b^\infty$$

where $b = -\infty$ for $j = 0$ and $b = 0$ for $j = 1$. The second term on the left can be integrated by parts using equation (B2) to obtain

$$\int_b^\infty Y^jV\frac{\partial U}{\partial Y}\,dY = \left(Y^jVU\right)_b^\infty + \int_b^\infty Y^jU\frac{\partial U}{\partial X}\,dY$$

Since τ and V vanish at the limits of integration, the momentum integral equals zero.

$$\frac{\partial}{\partial X}\int_b^\infty Y^jU^2\,dY = 0 \tag{B3}$$

We now introduce a similarity transformation

$$U = U_R x_m f(\eta), \qquad x = \frac{U_R X}{\nu}, \qquad y = \frac{U_R Y}{\nu}, \qquad \eta = \frac{y}{x^n} \tag{B4}$$

where U_R is a reference velocity. We may take the first term in equation (B1) as typical of inertia terms and find it to be

$$U \frac{\partial U}{\partial X} \equiv \frac{U_R^3}{\nu} x^{2m-1} f(mf - n\eta f') \tag{B5}$$

The stress term becomes

$$\frac{1}{Y^j} \frac{\partial}{\partial Y} \left(Y^j \frac{\tau}{\rho} \right) = \frac{\alpha U_R^3}{\nu} \frac{x^{2m-n}}{\eta^j} \frac{d}{d\eta} \left[\eta^j (f_m - f)(f - f_c) \right] \tag{B6}$$

where f_m and f_c correspond to U_m and U_c and we have assumed that f_c is independent of x.

Requiring equal powers of x in the inertia and stress terms (eqs. (B5) and (B6), respectively) yields

$$2m - 1 = 2m - n \tag{B7}$$

or $n = 1$. Thus, the similarity variable for both plane and circular jets is $\eta = y/x$.

The decay law for the centerline velocity is given by equation (B3):

$$\frac{\partial}{\partial x} x^{2m+(j+1)n} \int_b^\infty \eta^j f^2 \, d\eta = 0$$

The power of x in this expression must vanish under the constraint (B7) so that

$$m = -\frac{j + 1}{2}$$

or $m = -1/2$ for plane jets and $m = -1$ for circular jets.

Wakes

In this case we introduce the velocity deficit $U' = U_m - U$ and consider only the

wake far downstream, where U' is small compared with U_m. The similarity transformation (eq. (B4)) is again employed, with U replaced by U'. The typical inertia term becomes

$$U\frac{\partial U}{\partial X} = -\frac{U_m U_R^2}{\nu} x^{m-1}(mf - n\eta f')$$

and the stress term becomes

$$\alpha \frac{U_R^3}{\nu} x^{2m-n} \frac{1}{\eta^j} \frac{d}{d\eta}\left[\eta^j f(f_c - f)\right]$$

where it has been necessary to assume again that f_c can be considered constant. Equating powers of x in the inertia and stress terms yields $m - n = -1$.

Condition (B3) becomes for the wake

$$\frac{\partial}{\partial x} x^{m+(j+1)n} \int_b^\infty \eta^j f \, d\eta = 0$$

from which $m + (j + 1)n = 0$. The solutions of the conditions for m and n are

$$\left.\begin{aligned} m &= -\frac{1}{2} \\ n &= \frac{1}{2} \end{aligned}\right\} \quad \text{for plane wakes}$$

$$\left.\begin{aligned} m &= -\frac{2}{3} \\ n &= \frac{1}{3} \end{aligned}\right\} \quad \text{for circular wakes}$$

Half Jet or Mixing Layer

The equations of motion for a half jet or mixing layer are those for a plane jet. We take the lower fluid to be at rest and the upper fluid to have the constant, undisturbed

velocity U_m. The latter requirement forces m to equal 0 in equation (B4). Introducing this result into the comparison of inertia and stress terms in the plane-jet analysis yields $n = 1$.

APPENDIX C

N^{th} MOMENT EQUATION FOR FLAT-PLATE BOUNDARY LAYER

The integral of the n^{th} moment by $\delta - y$ of the dimensionless boundary-layer equation (31) with U_δ constant is

$$\int_0^\delta (\delta - y)^n \left(u \frac{\partial u}{\partial x} + v \frac{\partial u}{\partial y}\right) dy = \int_0^\delta (\delta - y)^n \frac{\partial}{\partial y}\left[\frac{1}{\alpha^2 \, \mathrm{Re}} \frac{\partial u}{\partial y} + (1 - u)(u - u_c)\right] dy \qquad (C1)$$

It is desired to transform this equation to a manifestly ordinary differential equation in x. Beginning with the second term on the left side, one has

$$\int_0^\delta (\delta - y)^n \, v \frac{\partial u}{\partial y} \, dy = \int_0^\delta (\delta - y)^n \frac{\partial (uv)}{\partial y} \, dy - \int_0^\delta (\delta - y)^n \, u \frac{\partial v}{\partial y} \, dy$$

$$= \int_0^\delta \frac{\partial}{\partial y}\left[(\delta - y)^n \, uv\right] dy + n \int_0^\delta uv(\delta - y)^{n-1} \, dy$$

$$+ \int_0^\delta (\delta - y)^n \, u \frac{\partial u}{\partial x} \, dy$$

$$= \delta_{n,0} v(\delta) + n \int_0^\delta (\delta - y)^{n-1} \, uv \, dy + \int_0^\delta (\delta - y)^n \, u \frac{\partial u}{\partial x} \, dy \qquad (C2)$$

The last term in equation (C2) is just equal to the first term in equation (C1) and their sum is

$$\int_0^\delta (\delta - y)^n \frac{\partial u^2}{\partial x} \, dy = \frac{d}{dx} \int_0^\delta (\delta - y)^n \, u^2 \, dy - \left[(\delta - y)^n \, u^2\right]_0^\delta \dot{\delta} - n\dot{\delta} \int_0^\delta (\delta - y)^{n-1} \, u^2 \, dy$$

$$= \frac{d}{dx} \int_0^\delta (\delta - y)^n \, u^2 \, dy - \delta_{n,0} \dot{\delta} - n\dot{\delta} \int_0^\delta (\delta - y)^{n-1} \, u^2 \, dy \qquad (C3)$$

On the right side of equation (C1) the first term is proportional to

$$\int_0^\delta (\delta - y)^n \frac{\partial^2 u}{\partial y^2}\, dy = \left[(\delta - y)^n \frac{\partial u}{\partial y}\right]_0^\delta + n \int_0^\delta \frac{\partial u}{\partial y} (\delta - y)^{n-1}\, dy$$

$$= - \delta^n \left(\frac{\partial u}{\partial y}\right)_0 + \delta_{n,1} + n(n-1) \int_0^\delta u(\delta - y)^{n-2}\, dy \qquad \text{(C4)}$$

and the second term is

$$\int_{y_c}^\delta (\delta - y)^n \frac{\partial}{\partial y} (1 - u)(u - u_c) dy = \left[(\delta - y)^n (1 - u)(u - u_c)\right]_{y_c}^\delta$$

$$+ n \int_{y_c}^\delta (\delta - y)^{n-1} (1 - u)(u - u_c) dy$$

$$= n \int_{y_c}^\delta (\delta - y)^{n-1} (1 - u)(u - u_c) dy \qquad \text{(C5)}$$

Combining equations (C2) to (C5) yields for the entire equation

$$\frac{d}{dx} \int_0^\delta (\delta - y)^n u^2\, dy - \delta_{n,0} \dot{\delta} - n\dot{\delta} \int_0^\delta (\delta - y)^{n-1} u^2\, dy + \delta_{n,0} v(\delta) + n \int_0^\delta (\delta - y)^{n-1} uv\, dy$$

$$= \left[- \delta^n \left(\frac{\partial u}{\partial y}\right)_0 + \delta_{n,1} + n(n-1) \int_0^\delta (\delta - y)^{n-2} u\, dy\right] \frac{1}{\alpha^2 \, Re}$$

$$+ n \int_{y_c}^\delta (\delta - y)^{n-1} (1 - u)(u - u_c) dy \qquad \text{(C6)}$$

Now consider, further, the case when the velocity profile is specified as a function of three parameters, one of which is the nominal boundary-layer thickness δ:

$$u = u(y; \delta, e, F) \tag{C7}$$

We can transform equation (C6) to an ordinary differential equation in δ, e, and F by introducing from the continuity equation

$$v(y) = - \int_0^y \frac{\partial u}{\partial x}\, dy = - \int_0^y \left(\frac{\partial u}{\partial \delta}\, \dot{\delta} + \frac{\partial u}{\partial e}\, \dot{e} + \frac{\partial u}{\partial F}\, \dot{F} \right) dy$$

and

$$v(\delta) = - \frac{d}{dx} \int_0^\delta u\, dy + \dot{\delta} = - \left[\dot{\delta}\, \frac{\partial}{\partial \delta} + \dot{e}\, \frac{\partial}{\partial e} + \dot{F}\, \frac{\partial}{\partial F} \right] \int_0^\delta u\, dy + \dot{\delta}$$

where $\dot{\delta} \equiv d\delta/dx$, and so forth. The coefficients of $\dot{\delta}$, $\dot{e}$, and $\dot{F}$ on the left side of equation (C6) are then, respectively,

$$A_{n1} = \frac{\partial}{\partial \delta} \int_0^\delta (\delta - y)^n u^2\, dy - n \int_0^\delta (\delta - y)^{n-1} u^2\, dy - \delta_{n,0} \frac{\partial}{\partial \delta} \int_0^\delta u\, dy$$

$$- n \int_0^\delta (\delta - y)^{n-1} u \int_0^y \frac{\partial u}{\partial \delta}\, dy'\, dy \tag{C8a}$$

$$A_{n2} = \frac{\partial}{\partial e} \int_0^\delta (\delta - y)^n u^2\, dy - \delta_{n,0} \frac{\partial}{\partial e} \int_0^\delta u\, dy - n \int_0^\delta (\delta - y)^{n-1} u \int_0^y \frac{\partial u}{\partial e}\, dy'\, dy \tag{C8b}$$

$$A_{n3} = \frac{\partial}{\partial F} \int_0^\delta (\delta - y)^n u^2\, dy - \delta_{n,0} \frac{\partial}{\partial F} \int_0^\delta u\, dy$$

$$- n \int_0^\delta (\delta - y)^{n-1} u \int_0^y \frac{\partial u}{\partial F}\, dy'\, dy \qquad n = 0, 1, 2 \ldots \tag{C8c}$$

With the further definition for the right side of equation (C6), namely,

$$B_n = \frac{1}{\alpha^2 \, Re}\left[\delta_{n1} - \delta^n \left(\frac{\partial u}{\partial y}\right)_0 + n(n-1)\int_0^\delta (\delta - y)^{n-2}\, u\, dy\right]$$

$$+ n\int_{y_c}^{\delta} (\delta - y)^{n-1}(1-u)(u-u_c)dy \qquad \text{(C8d)}$$

we can rewrite equation (C6) in the desired form of an explicitly ordinary differential equation

$$A_{n1}\dot{\delta} + A_{n2}\dot{e} + A_{n3}\dot{F} = B_n$$

In principle, any set of three of these equations may be used to solve for δ, e, and F. In practice, the simplest to use will be the first three: $n = 0, 1, 2$.

APPENDIX D

MATRIX COEFFICIENTS AND INITIAL CONDITIONS FOR POWER-LAW VELOCITY PROFILE

We assume the velocity is described by

$$u = \frac{F^2}{J} y \qquad \text{for } 0 < u < u_c \tag{42}$$

$$u = \left(\frac{y}{\delta}\right)^{1/e} \qquad \text{for } u_c < u < 1 \tag{D1}$$

The coordinate at the partitioning velocity is

$$y_c = \frac{J}{F} \tag{40}$$

and the relation between the parameters δ, e, and F resulting from the matching at $u = u_c$ is

$$\delta = \frac{J}{F^{1+e}} \tag{43}$$

The dimensionless displacement thickness

$$\frac{\Delta^*}{\alpha L} \equiv \delta^* = \int_0^{\delta} (1 - u)dy = \int_0^{y_c} \left(1 - \frac{F^2}{J} y\right)dy + \int_{y_c}^{\delta} \left[1 - \left(\frac{y}{\delta}\right)^{1/e}\right]dy$$

$$= J\left[\frac{1}{e + 1}\left(e + \frac{1}{F^{1+e}}\right) - \frac{1}{2}\right]$$

Similarly, the dimensionless momentum thickness is

$$\frac{\Theta}{\alpha L} \equiv \theta = \int_0^{\delta} u(1 - u)dy = J\left\{\frac{1}{2} - \frac{F}{3} + \frac{1}{F^{1+e}}\left[\frac{e}{e + 1}(1 - F^{e+1}) - \frac{e}{e + 2}(1 - F^{e+2})\right]\right\}$$

The coefficients appearing in the first two integral moment equations are obtained by substituting the velocity specifications (42) and (D1) into equation (C8), performing the integrals, replacing y_c with equation (40), and then performing the differentiations with respect to δ, e, and F with J held constant. In terms of the definitions $z = y_c/\delta = J/F\delta$, $z_1 = z^{1/(e+1)}$, $z_2 = z^{2/(e+1)}$, and $z_3 = 1 - z_1$, the coefficients are

$$A_{01} = z_1 - z_2 + \frac{e}{e+1}(1 - z_1) - \frac{e}{2+e}(1 - z_2)$$

$$A_{02} = \delta\left[\frac{1 - z_1}{(e+1)^2} + \frac{z_1 \ln z}{e(e+1)} - \frac{2(1 - z_2)}{(2+e)^2} - \frac{2z_2 \ln z}{e(2+e)}\right]$$

$$A_{03} = \frac{\delta}{F}(z_1 - z_2) - \frac{J}{3}$$

$$B_0 = \frac{F^2}{\alpha^2 J\, Re}$$

$$A_{11} = \delta e\left\{\frac{1 - z_2}{e+2} + \frac{1 - z_1}{e+1}\left[\frac{1 - z_1}{2(e+1)} - (1 + z_1)\right]\right\} + \delta\left(z_2 - z_1^2\right)$$

$$A_{12} = \delta^2\left[\frac{2(1 - z_2)}{(e+2)^2} - \frac{1 - z_1^2}{2(e+1)^2}\right] + \delta^2\left(\frac{2z_2}{2+e} - \frac{z_1^2}{1+e}\right)\frac{\ln z}{e}$$

$$- \frac{\delta^2}{(e+1)^2}\left[\left(z_1 - \frac{z_1^2}{2}\right)\ln z + \frac{e}{e+1}(2 + z_3)\frac{z_3}{4}\right]$$

$$A_{13} = \frac{J\delta}{3} + \frac{\delta^2}{F}\left(z_2 - z_1^2\right) - \frac{J}{F}\left[\frac{J}{4} + \frac{e\delta(1 - z_1)}{e+1}\right]$$

$$B_1 = \frac{1}{\alpha^2\, Re}\left(1 - \frac{\delta F^2}{J}\right) - \delta\left[\frac{e(1 - z_2)}{2+e} - \frac{e(1+F)(1 - z_1)}{e+1} + F(1 - z)\right]$$

A third differential relation between δ, e, and F is obtained by differentiating equation (43). After multiplication by δ, the coefficients are

$$A_{21} = 1$$

$$A_{22} = \delta \ln F$$

$$A_{23} = \frac{\delta}{F} (e + 1)$$

$$B_2 = 0$$

APPENDIX E

MATRIX COEFFICIENTS AND INITIAL CONDITIONS FOR THE THREE-PARAMETER PROFILE

If the velocity profile defined by equations (47) and (48) is used to evaluate the coefficients defined in equation (C8), they can be written as follows:

$$A_{01} = S_1 + (\delta - y_c)\frac{F^2 S_2}{3J(e - 1)}$$

$$A_{02} = c(\delta - y_c)\left(3S_3 - \frac{S_2}{e - 1}\right)$$

$$A_{03} = -\frac{J}{3} + \frac{JS_1}{F^2} + (\delta - y_c)(S_2 c_F - S_4)$$

$$B_0 = \frac{1}{\alpha^2 \, Re}\frac{F^2}{J}$$

$$A_{11} = (\delta - y_c)\left[2C_7 - C_8 - S_1 + (1 - F)C_1 + C_{17}\right] + (\delta - y_c)^2 c_\delta C_9$$

$$A_{12} = (\delta - y_c)^2\left[3cC_3\left(2 + \frac{1}{3e + 1}\right) - \frac{3c(C_1 - C_4)}{(3e + 1)^2} + C_9 c_e\right]$$

$$A_{13} = J\left[\frac{\delta}{3} + \frac{\delta - y_c}{F^2}(C_{17} + 2C_7)\right] - \left(\frac{y_c}{2}\right)^2 F - y_c(\delta - y_c)C_1 + (\delta - y_c)^2\left(2C_2 - \frac{C_1 - C_2}{4} + c_F C_9\right)$$

$$B_1 = \frac{1}{\alpha^2 \, Re}\left(1 - \frac{F^2\delta}{J}\right) + (\delta - y_c)\left[(1 - F)S_{11} - S_{12}\right]$$

$$A_{21} = (\delta - y_c)^2\left[C_{10} - 1 + 2(1 - F)C_{14} + 2C_{71} - 2C_{18}\right]$$

$$A_{22} = (\delta - y_c)^3\left\{\frac{2}{3}cC_{13} - \frac{2c}{(3e+1)^2}\left[3C_{14} - \frac{(3e+1)C_{13}}{3} - C_{11}\right] + c_e C_{16}\right\}$$

$$A_{23} = J\left(\frac{\delta^2}{3} - \frac{\delta y_c}{2} + \frac{y_c^2}{5}\right) + (\delta - y_c)^2 y_c\left(\frac{C_{10} - 2C_{18}}{F} - 2C_{14}\right) + (\delta - y_c)^3\left(\frac{5C_{12}}{12} - \frac{C_{14}}{2} + c_F C_{16}\right)$$

$$B_2 = \frac{1}{\alpha^2\,\mathrm{Re}}\left[-\frac{\delta^2 F^2}{J} + J + 2(\delta - y_c)C_1\right] + 2(\delta - y_c)^2\left[(1 - F)C_{71} - C_{72}\right]$$

In these expressions for the matrix coefficients the following groupings have been used: $y_c = J/F$, $c = \left[(\delta - y_c)F^2/3J - 1 + F\right]/(e - 1)$, and $b = 1 - F - c$

$$S_{11} = \frac{b}{4} + \frac{c}{3e+1}$$

$$S_{12} = \frac{b^2}{7} + \frac{2bc}{3e+4} + \frac{c^2}{6e+1}$$

$$S_1 = S_{11} - S_{12}$$

$$S_{21} = \frac{1}{3e+1} - \frac{1}{4}$$

$$S_2 = S_{21} + 2\left(\frac{b}{7} + \frac{c-b}{3e+4} - \frac{c}{6e+1}\right)$$

$$S_3 = -\frac{1}{(3e+1)^2} + \frac{2b}{(3e+4)^2} + \frac{2c}{(6e+1)^2}$$

$$S_4 = \frac{1}{4} - 2\left(\frac{b}{7} + \frac{c}{3e+4}\right)$$

$$C_1 = 1 - \frac{b}{4} - \frac{c}{3e+1}$$

$$C_2 = \frac{1}{5} - \frac{b}{8} - \frac{c}{3e+5}$$

$$C_3 = \frac{1}{(3e+2)^2} - \frac{b}{(3e+5)^2} - \frac{c}{(6e+2)^2}$$

$$C_4 = \frac{1}{3e+2} - \frac{1}{3e+5} - \frac{c}{6e+2}$$

$$C_5 = \frac{1}{4} - \frac{1}{3e+1}$$

$$C_6 = C_5 C_1 + \frac{C_4}{3e+1} - \frac{C_2}{4}$$

$$C_{71} = \frac{b}{5} + \frac{c}{3e+2}$$

$$C_{72} = \frac{b^2}{8} + \frac{2bc}{3e+5} + \frac{c^2}{6e+2}$$

$$C_7 = \frac{1}{2} - 2C_{71} + C_{72}$$

$$C_8 = 1 + 2(C_1 - 1) + S_{12}$$

$$C_9 = 2C_2 - 2C_4 - C_6$$

$$C_{10} = 1 - b - \frac{2c}{e+1} + \frac{b^2}{3} + \frac{2bc}{e+2} + \frac{c^2}{2e+1}$$

$$C_{11} = \frac{1}{e+1} - \frac{b}{e+2} - \frac{c}{2e+1}$$

$$C_{12} = 1 - \frac{2b}{3} - \frac{2c}{e+2}$$

$$C_{13} = \frac{1}{(e+1)^2} - \frac{b}{(e+2)^2} - \frac{c}{(2e+1)^2}$$

$$C_{14} = \frac{1}{2} - \frac{b}{5} - \frac{c}{3e + 2}$$

$$C_{15} = C_5 C_{14} + \frac{1}{3e + 1}\frac{C_{11}}{3} - \frac{C_{12}}{24}$$

$$C_{16} = \frac{C_{12} - 2C_{11}}{3} - 2C_{15}$$

$$C_{191} = \frac{b}{4}$$

$$C_{192} = \frac{ec}{3e + 1}$$

$$C_{19} = C_{191} + C_{192}$$

$$C_{17} = 3(-C_{19}C_1 + C_{191}C_2 + C_{192}C_4)$$

$$C_{18} = 3C_{19}C_{14} - \frac{1}{2} C_{191}C_{12} - C_{192}C_{11}$$

$$c_\delta = \frac{F^2}{3J(e - 1)}$$

$$c_e = \frac{-c}{e - 1}$$

$$c_F = \frac{2}{3} \frac{\left(\frac{\delta}{y_c} + 1\right)}{e - 1}$$

If Δ^* and Θ are the initial values of the dimensional displacement and momentum-loss thicknesses, and if f is the initial value of the friction coefficient, the corresponding initial values of the parameters δ, e, and F are obtained by calculating displacement thickness, momentum-loss thickness, and friction coefficient from the profiles in equation (19) and equating them to the experimental values. The result is a set of three equations

$$F = u_c^+ \sqrt{\frac{f}{2}}$$

$$J\left(\frac{1}{F} - \frac{1}{2}\right) + (\delta - y_c)S_{11} = \frac{\Delta^*}{\alpha L}$$

$$J\left(\frac{1}{F} - 1 + \frac{F}{3}\right) + (\delta - y_c)S_{12} = \frac{\Delta^* - \Theta}{\alpha L}$$

for δ, e, and F.

REFERENCES

1. Reynolds, W. C.: Computation of Turbulent Flows. Annual Review of Fluid Mechanics, vol. 8, M. VanDyke and W. G. Vincenti, eds., Annual Reviews, Inc., 1976, pp. 183-208.

2. Launder, B. E.; and Spalding, D. B.: Lectures in Mathematical Models of Turbulence. Academic Press, 1972.

3. Townsend, A. A.: The Structure of Turbulent Shear Flow. Cambridge Univ. Press, 1956.

4. Tennekes, H.; and Lumley, J. L.: A First Course in Turbulence. The MIT Press, 1972, pp. 41-50.

5. Chevray, René; and Kovasznay, Leslie S. A.: Turbulence Measurements in the Wake of a Thin Flat Plate. AIAA J., vol. 7, no. 8, Aug. 1969, pp. 1641-1643.

6. Free Turbulent Shear Flows, Vol. II - Summary of Data. NASA SP-321, 1972.

7. Deissler, Robert G.: Analysis of Turbulent Heat Transfer, Mass Transfer, and Friction in Smooth Tubes at High Prandtl and Schmidt Numbers. NACA TR 1210, 1955.

8. van Driest, E. R.: On Turbulent Flow Near a Wall. J. Aeronaut. Sci., vol. 23, no. 11, Nov. 1956, pp. 1007-1011, 1036.

9. Schlicting, Hermann (J. Kestin, transl.): Boundary Layer Theory. Fourth ed. McGraw-Hill Book Co., Inc., 1960.

10. Townsend, A. A.: The Structure of the Turbulent Boundary Layer. Proc. Cambridge Philos. Soc., vol. 47, pt. 2, Apr. 1950, pp. 375-395.

11. Goldstein, Marvin E.; and Braun, Willis H.: Advanced Methods for the Solution of Differential Equations. NASA SP-316, 1973.

12. Abramowitz, Milton; and Stegun, Irene A., eds.: Handbook of Mathematical Functions with Formulas, Graphs and Mathematical Tables. Natl. Bur. Stand. Applied Mathematics Series 55. U. S. Government Printing Office, 1964.

13. Laufer, John: Some Recent Measurements in a Two-Dimensional Turbulent Channel. J. Aeronaut. Sci., vol. 17, no. 5, May 1950, pp. 277-287. (See also NACA TN 2123 and NACA TR 1053.)

14. Laufer, John: The Structure of Turbulence in Fully Developed Pipe Flow. NACA TR 1174, 1954.

15. Sandborn, Virgil A.: Experimental Evaluation of Momentum Terms in Turbulent Pipe Flow. NACA TN 3266, 1955.

16. Walz, A. (Hans Joerg Oser, transl.): Boundary Layers of Flow and Temperature. The MIT Press, 1969.

17. Tetervin, Neal; and Lin, Chia Chiao: A General Integral Form of the Boundary Layer Equation for Incompressible Flow with an Application to the Calculation of the Separation Point of Turbulent Boundary Layers. NACA TR 1046, 1951.

18. Coles, D. E.; and Hirst, E. A., eds.: Proceedings, Computation of Turbulent Boundary Layers, 1968 AFOSR-IFP-Stanford Conference, Volume II, Compiled Data. Stanford University, 1969.

19. Pai, S. I.: On Turbulent Flow Between Parallel Plates. J. Appl. Mech., vol. 20, no. 1, Mar. 1953, pp. 109-114.

20. Pai, S. I.: On Turbulent Flow in Circular Pipe. J. Franklin Inst., vol. 256, no. 4, Oct. 1953, pp. 337-352.

21. Sandborn, V. A.: An Approximate Equation for the Mean Velocity Distribution in an Incompressible Turbulent Boundary Layer. Proceedings of the Fifth Midwestern Conference on Fluid Mechanics. Univ. Michigan Press, 1957, pp. 85-107.

22. Klebanoff, P. S.: Characteristics of Turbulence in a Boundary Layer with Zero Pressure Gradient. NACA TN 3178, 1954.

23. Liepmann, Hans Wolfgang; and Laufer, John: Investigations of Free Turbulent Mixing. NACA TN 1257, 1947.

24. Sandborn, Virgil A.; and Braun, Willis H.: Turbulent Shear Spectra and Local Isotropy in the Low-Speed Boundary Layer. NACA TN 3761, 1956.

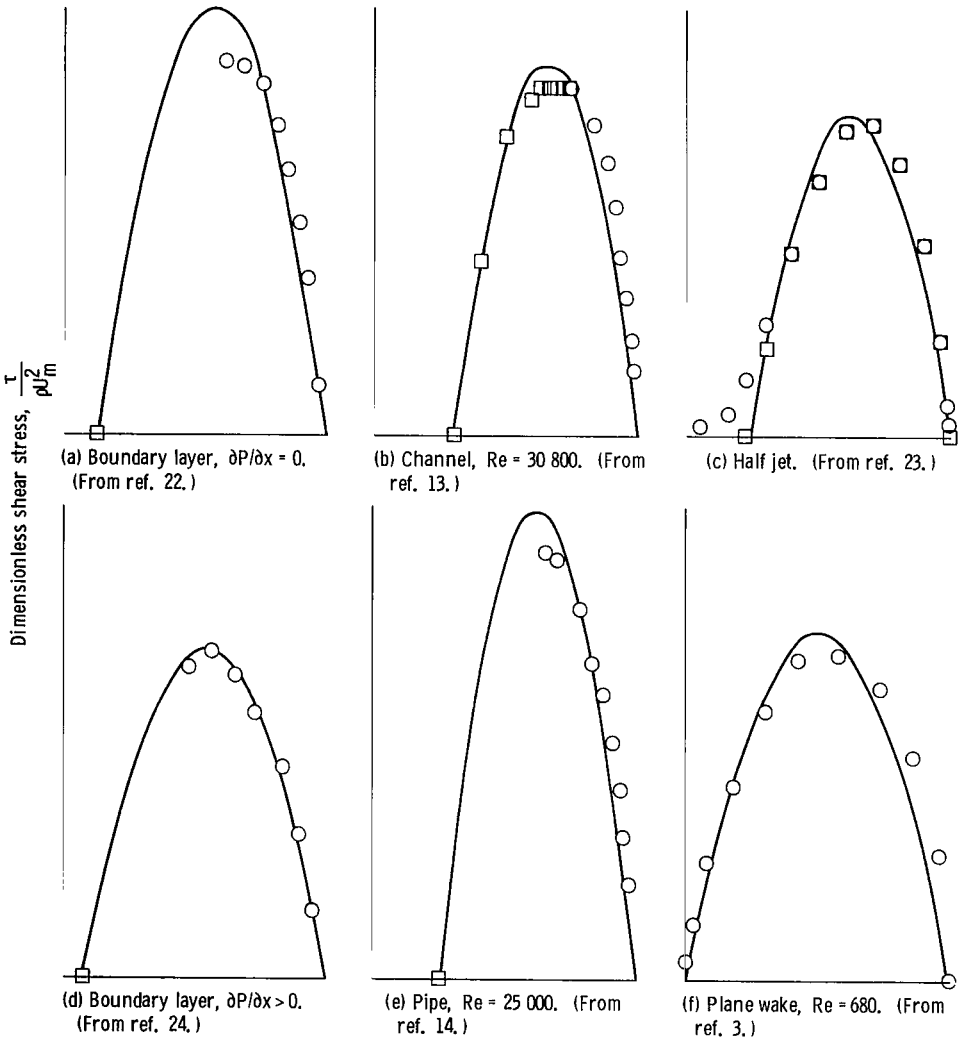

Figure 1. - Turbulent shear-stress distributions (varying scales).

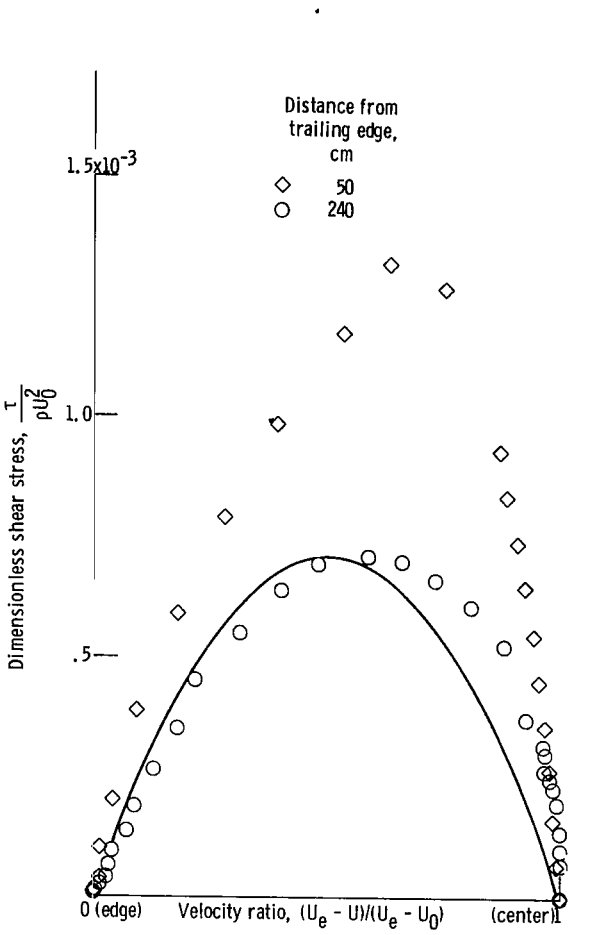

Figure 2. - Shear-stress distributions in wake of a plate. (From refs. 5 and 6.)

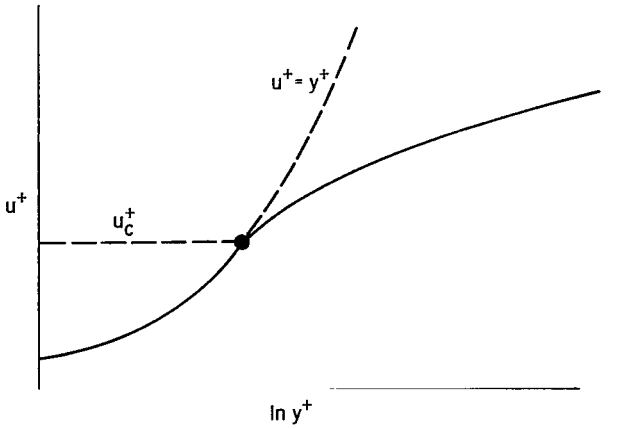

Figure 3. - Method of specifying cutoff velocity.

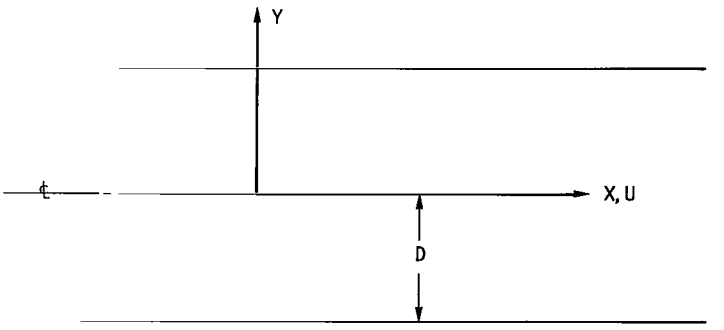

Figure 4. - Channel coordinates.

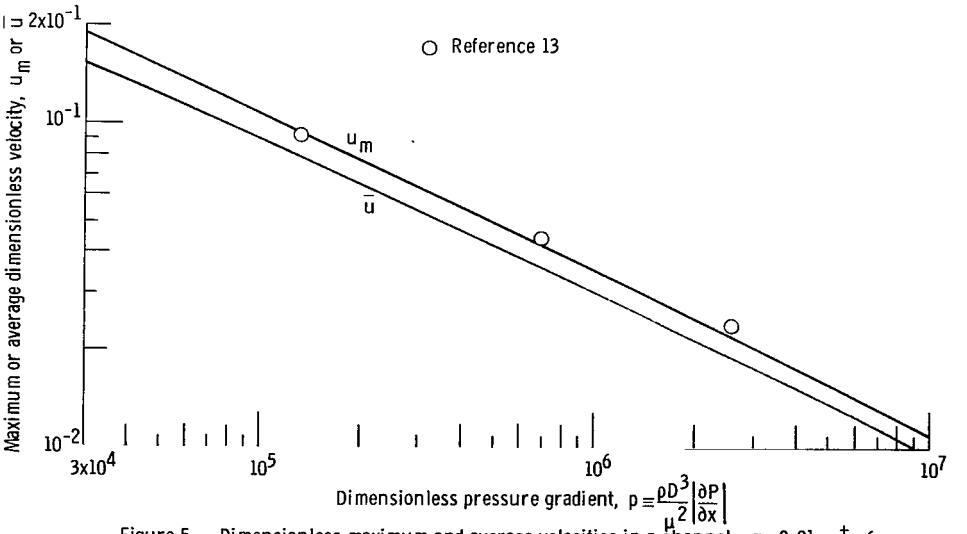

Figure 5. - Dimensionless maximum and average velocities in a channel. $\alpha = 0.01$; $u_c^+ = 6$.

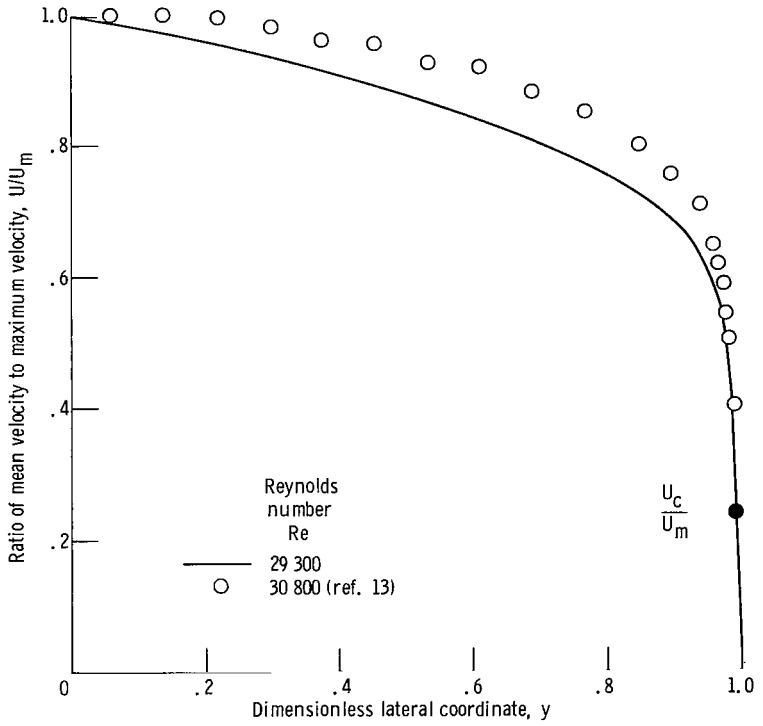

Figure 6. - Velocity distribution across a channel. $\alpha = 0.01$; $u_c^+ = 6$.

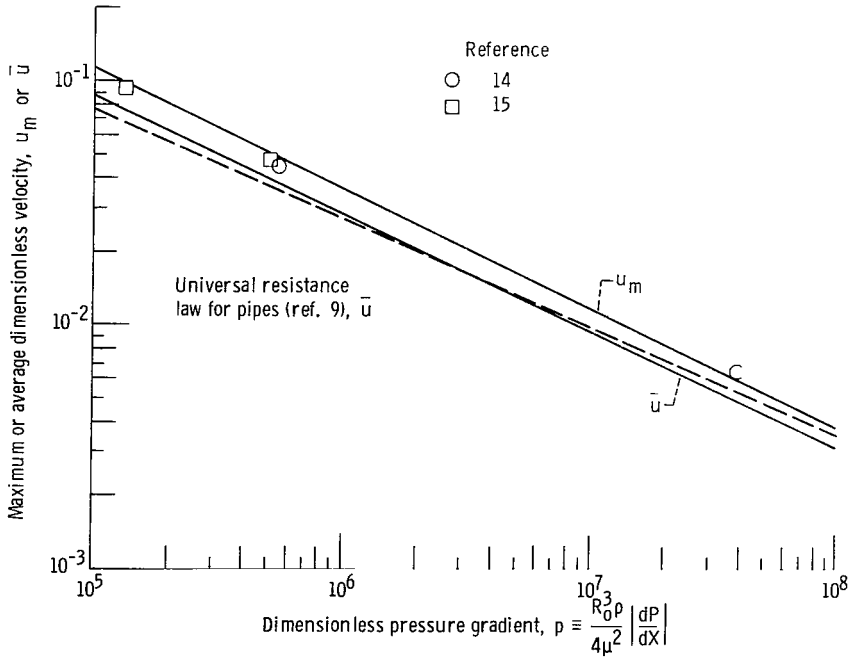

Figure 7. - Maximum and average velocities in a pipe. $\alpha = 0.01$; $u_c^+ = 7$.

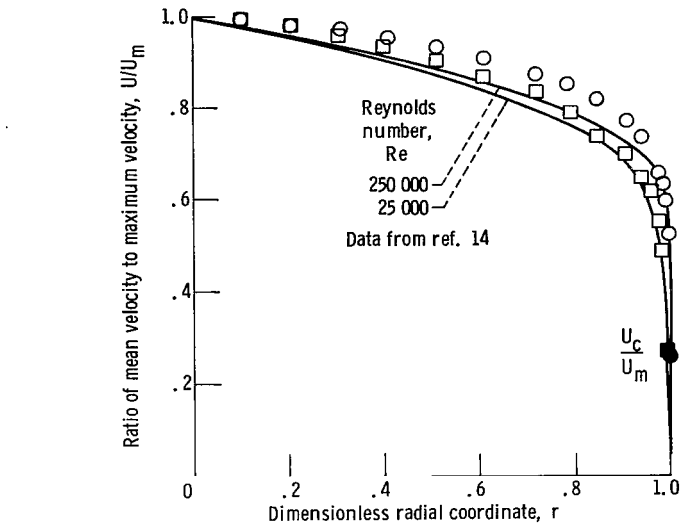

(a) Normalized coordinates.

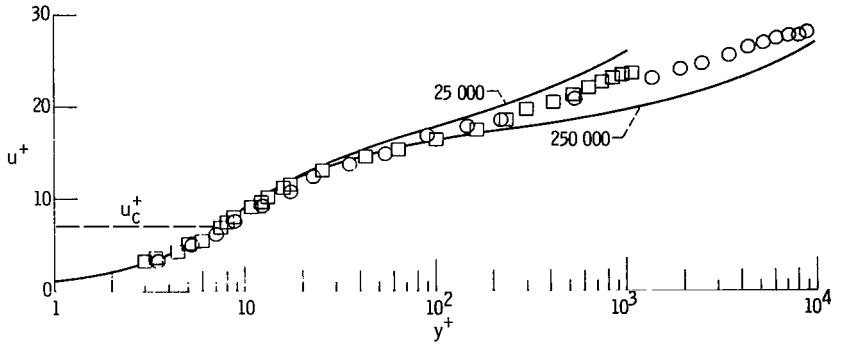

(b) Similarity variables.

Figure 8. - Velocity distribution in a pipe. $\alpha = 0.01$; $u_c^+ = 7$.

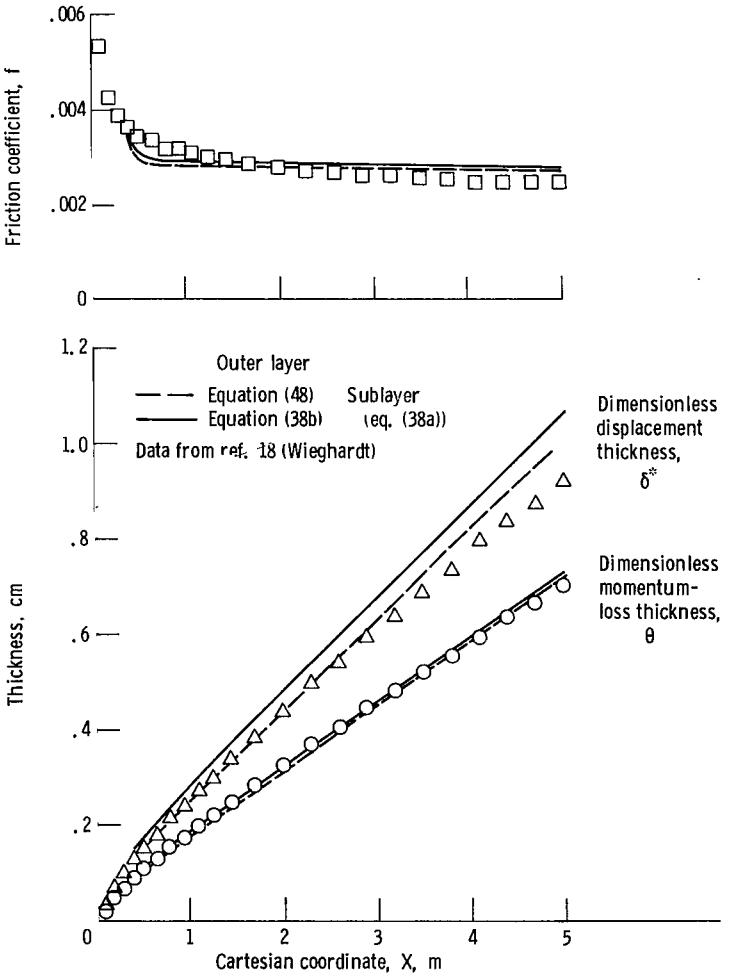

Figure 9. - Friction coefficient, displacement thickness, and momentum loss thickness in a flat-plate boundary layer.

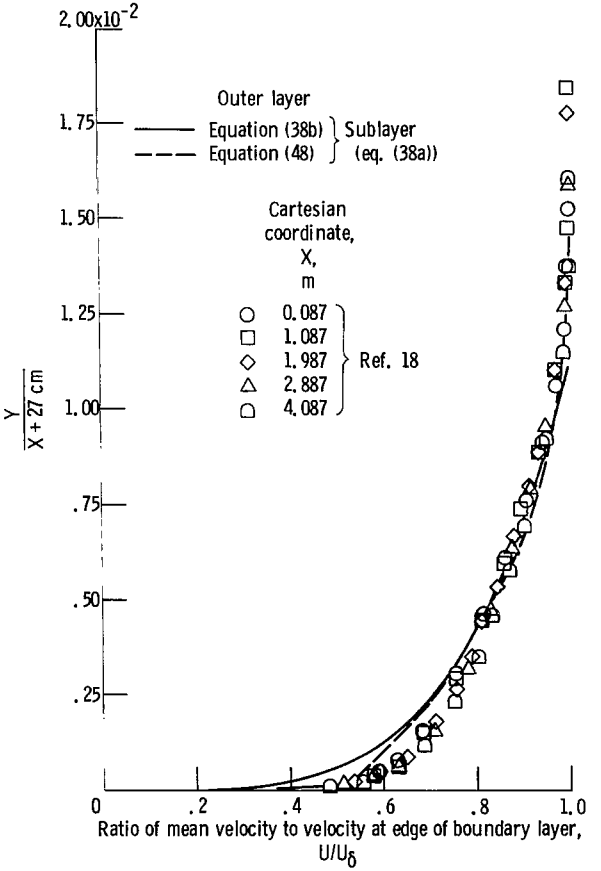

Figure 10. - Velocity profiles in a flat-plate boundary layer.

National Aeronautics and
Space Administration

Washington, D.C.
20546

Official Business
Penalty for Private Use, $300

THIRD-CLASS BULK RATE

Postage and Fees Paid
National Aeronautics and
Space Administration
NASA-451

588 001 C1 U D 770819 S00903DS
DEPT OF THE AIR FORCE
AF WEAPONS LABORATORY
ATTN: TECHNICAL LIBRARY (SUL)
KIRTLAND AFB NM 87117

NASA

POSTMASTER: If Undeliverable (Section 158 Postal Manual) Do Not Return